Design of Air Bearing for High Speed Micro Gas Turbine

M.Muruganandam,
Student, Thermal Engineering Branch,
Government College of Technology,
Coimbatore – 641 013, Tamil Nadu.
E-mail:muruganandammma@yahoo.co.in.
Mr.S.Nadarajan,
Selection Grade Lecturer, Mechanical Engineering Department,
Government College of Technology,
Coimbatore – 641 013.
E-mail:nadarajan.s@rediffmail.com,
Ph.No:2432221 Extn:362.
Dr.S.Ramamurthy.
Scientist, Propulsion Division,
National Aerospace Laboratories,
Bangalore – 560 017,
E-mail:ramamurthy_srm@yahoo.com,
Ph.No:080-25051705, 25057787.

Abstract

This paper deals with the design and analysis of air bearing suitable for high speed micro gas turbine. Design has been carried out for a turbine rotor having symmetrical loading by mathematical modeling and numerical simulation of its dynamic motion. The rigid symmetrical rotor is supported in two air bearings and each bearing is of radial configuration with a cylindrical bush. The input parameters from the micro gas turbine design have been considered for the design of bearing to suit the rotor system. For the established shaft configuration, non-linear Reynolds equation is solved to get the air pressure distribution in the gap between the shaft and the bush. The load capacity of the bearing is calculated by integrating the pressure distribution obtained earlier. The displacements, velocities and dynamic components of load capacity with time are used to evaluate the damping and stiffness coefficients of air film between the journal and the bush. A non-linear equation of motion of the shaft is evolved using the above coefficients. The stability threshold is estimated from the linearized equations of motion. The stability threshold estimation leads to arrival of stability boundaries of rotor bearing system characterized by the required stiffness and damping coefficients of the bush support surrounding the air bearing. The required stiffness and damping coefficients of bush are achieved by providing an air ring around the bush. The complete mathematical procedure has been coded using MATLAB Software.

Symbols

a amplitude of kinematically forced harmonic motion of the shaft
A_d ($=\pi r_d^2$), A_k ($=2\pi r_0 h$) areas of cross section of orifice ($_d$), feedhole ($_k$), m^2
C^o dimensionless constant
C_{ij} damping coefficients of gas film
C_p damping coefficient of elastic support

c radial clearance, m
c_1 clearance between the journal and the inner bush (air bearing).
c_2 clearance between the inner bush and the outer bush (air ring).
e_x, e_y coordinates of static equilibrium position of the shaft
F load capacity of the bearing
F_{ii} dynamic forces in gas film
F_{Ci}, F_{Ki}, dynamic forces in the support
F_z static loading of bearing
FK_1, FK_2, FK_3, dimensionless constants
F_x, F_y, F_{xx}, F_{yx}, F_{xy}, F_{yy}, dynamic components of load capacity F
h local film thickness, m
h_k height of chamber, m
H dimensionless film thickness
K_{ij} stiffness coefficients of bearing
K_p stiffness coefficient of elastic support
L length of bearing, m
m_d, m_k mass flow through orifice($_d$), feedhole($_k$), kg/s
m_d, m_k critical mass flow through orifice($_d$), feedhole($_k$), kg/s
P dimensionless pressure in the gap shaft bush
p_a atmospheric pressure, Pa
p_0 supply pressure, Pa
p_1 pressure in the chambers, Pa
Q ($=P^2$) dimensionless variable
Q mean value of Q
R radius of bearing, m
R_1 radius of journal.
R_2 outer radius of inner bush.
$\Re$ universal gas constant, J/kg K
Re Reynolds Number
r_0 radius of plain feedhole, m
r_d radius of orifice, m
t time, s
T period of vibrations
T_0 constant air temperature, K
V volume of chamber, m^3
x, y displacements of mass center of rotor
β critical pressure ratio
ρ_a air density at the atmospheric pressure, kgm^{-3}
σ air viscosity, Nsm^{-1}
ε relative eccentricity
θ_s angle between displacement and force
θ, ξ dimensionless coordinates of air film
κ isentropic expansion index
Λ dimensionless bearing number
υ_d, υ_k dimensionless mass flow through orifice ($_d$), feedhole ($_k$)
π_d ($=p_1/p_0$), π_0 ($=p_0/p_a$) pressure ratios
ν angular frequency of vibrations
τ ($=\nu t/2\Lambda$) dimensional time
ω angular velocity of shaft, rad/s.

Introduction

Since 1960, Gas bearings have been used to support rotors in machines. They have been designed for several applications, including gyros, supports for magnetic heads in computer hard disc, low-temperature equipment, heat pump, injection system in automobiles, grinding machines (Toshiba), gas turbines, compressors and special machine tools. Gas bearings are particularly valuable when they are used to support high-speed rotors in precision machines. Gas-lubricated films are nearly isothermal, because the ability of the bearing materials to dissipate heat is greater than the heat-generating capacity of gas films, which have very low friction losses, so no thermal effects appear during gas bearing operation. These advantages of gas bearings are due to the fact that the surfaces of the journal and bush are separated by a gas (mainly air) layer characterized by a very low (compared with oil) viscosity. Gas bearings retain their advantages at high rotational velocities, which significantly exceed the maximum rotational velocities admissible for oil bearings and rolling bearings.

The major obstacle to widespread application of gas bearings has been the phenomenon of a self-excited whirl, which is more prominent than in liquid-lubricated bearings. It makes them unstable and limits their range of applications. Two major kinds of instabilities are possible in gas bearings. The first kind of instability is associated with typical spring-mass natural frequencies, where the bearing gas film is the spring. As with usual spring-mass resonance, it is possible to have stability on either side of the critical speed, which corresponds to a natural frequency. The second kind of instability is a self-excited vibration characterized by a frequency equal to or less than half of the rotational velocity of the shaft. The shaft may be stable as the speed is increased until the stability threshold is reached. After crossing this threshold a further increase in speed will result in loss of damping properties of the gas film, which will make the system unstable. The second kind of instability under given operating conditions is one of the most important considerations in designing a high-speed, gas-lubricated journal bearing, because the amplitude of self-excited vibrations quickly exceeds the maximum value determined by the bearing clearance and shaft-bush eccentricity, which leads to contact between the journals and the bushes and destruction of the rotor and the bearings [1].

There have been many attempts to raise the stability threshold of gas bearings. Most of these attempts involve new designs of bearings, such as partial arc bearings and porous bearings. One

efficient way to improve the stability of gas bearings is to use an elastic support for the bush. Many investigations, reported in numerous papers, have used this method to try to raise the critical value of the rotational velocity. They have demonstrated that proper selection of the values of stiffness and damping coefficients of the elastic bush support leads to a vanishing unstable regions, that is, elimination of the phenomenon of self-excited vibrations. Professor Krzysztof Czolczynski has presented a methodology by which it is possible to design a real construction supporting the bushes that are characterized by the required values of the stiffness and damping coefficients and has, at the same time, high enough load capacity [2]. Elastic supports can be designed as a gas ring surrounding the bush. The bearing bush does not rotate, so this bush must be externally pressurized. In a book published by the same author on "Rotor Dynamics of Gas-Lubricated Journal Bearing Systems", presented the results of trials to eliminate the self-excited vibrations from the system in which the rotor is supported in self-acting or externally pressurized bearing. This paper attempts to use this procedure for designing an externally pressurized air bearing for a rotor having mass of 200gm and journal diameter of 10mm.

Air Journal Bearing Mathematical Modeling and Simulation of its motion

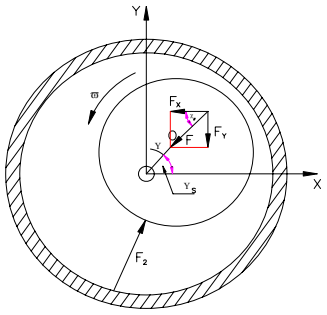

Fig. 1 Air Bearing

The object of considerations is a radial, externally pressurized air bearing with a cylindrical bush, as shown in Fig. 1. The description of the bearing is given in the system of Cartesian coordinates (x-y-z) related to the bush; the force F_z means the external loading of the journal and F is the load capacity.

Input parameters considered for the design of air bearing are –
Mass of rotor system = 200 gram.
Mass of the joint bushing = 50 gram.
Distance between journal centers = 95 mm.
Journal diameter = 10 mm.
Journal length = 8 mm.
Radial clearance = 3 to 30 micron.
Air viscosity = 18.2 x 10^{-06} Kg m^{-1} s^{-1}.
Air supply pressure = 2.026 bar.
Maximum speed of rotor = 1, 00,000 rpm.
Mass moment of inertial of rotor[1] = 2.1568 x 10^{-04} Kg-m^2.
Mass moment of inertial of joint bush[2] = 1.1649 x 10^{-04} Kg-m^2.

Air Bearing Assembly – The externally pressurized air bearing assembly is shown in Fig. 2 where the following parts are identified. (1) Rotor, (2) inner bush, (3) rubber longitudinal baffle, (4) casing (outer bush), (5) feedholes. The chamber feeding system of an air bearing (part no. 5 in Fig. 2) is shown in Fig. 3. The air at pressure p_0 flows through the orifices with the cross-sectional area A_d to the chambers of the volume V and then through the feedholes of the radius r_0 to the gap between the journal and the bearing bush.

To describe the mass flow through the feed system, it is necessary to formulate [1], [3], [4]:

1. The simplified relation between the mass flow through a feedhole of the radius r_0 and the air film pressure distribution surrounding the feedhole;
2. The relation between a mass flow and a pressure drop for the feedhole of the cross-section A_k;
3. the relation between a mass flow and a pressure drop for the orifice of the cross-section A_d; and
4. the equations of continuity using the relations specified in 1-3.

From the above relations the eq (1) and eq (2) are arrived at.

$$[1-K(1-\beta)(A)]^2\,\pi_d^2\,\pi_o^2 = B$$

where

$$A = 1-\sqrt{1-\upsilon_k^2}$$

$$B = \overline{Q} + \frac{\upsilon_k \pi_d}{H^2} F K_1$$

$$K = 0.16 + 0.0002\,\mathrm{Re}\ \textit{for}\ \mathrm{Re} \le 2000$$

$$K = 0.685 + 0.155y - 0.19y^2\ \textit{for}\ 2000 \le \mathrm{Re} \le 4000 \qquad (1)$$

$$y = \frac{\mathrm{Re}-3000}{2000}$$

$$K = 0.715\ \textit{for}\ \mathrm{Re} \ge 4000$$

$$\upsilon_d A_d - \upsilon_k A_k \pi_d = (\pi_d - \pi_{do})\frac{V}{\Delta t} F K_3 \qquad (2)$$

[1], [2]. About an axis perpendicular to spin axis and passing through its center of gravity

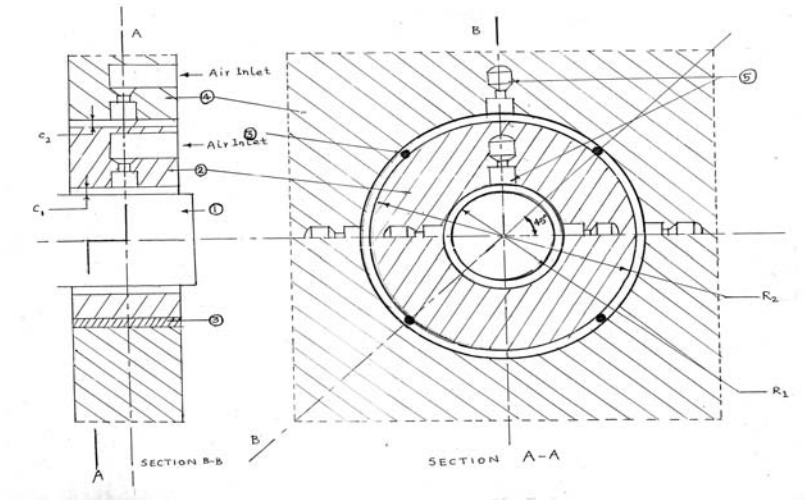

Fig. 2 Air Bearing Assembly

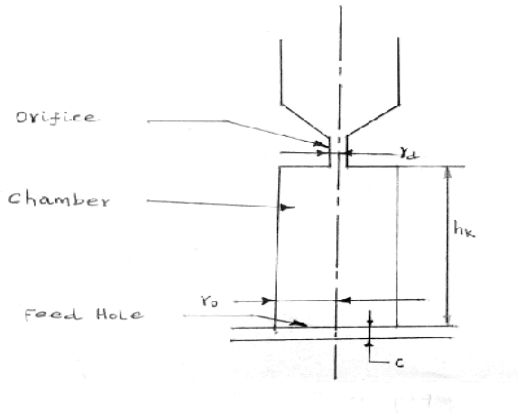

Fig. 3 Air Feed Hole Geometry

where

$$FK_3 = \frac{1}{\Re T_o \sqrt{\frac{2\kappa}{(\kappa-1)\Re T_o}\left(1-\beta^{\frac{\kappa-1}{\kappa}}\right)}} \frac{1}{\beta^{\frac{1}{\kappa}}}$$

The Reynolds equation, which describes the pressure distribution in the bearing gap, is eq (3).

$$-\frac{\partial}{R\partial\theta}\left(\frac{\rho h^3}{\sigma}\frac{\partial p}{R\partial\theta}\right)-\frac{\partial}{\partial z}\left(\frac{\rho h^3}{\sigma}\frac{\partial p}{\partial z}\right)+12\frac{\partial}{\partial t}(\rho h)+$$
$$6\omega\frac{\partial}{\partial\theta}(\rho h)=0$$
$$-\frac{\partial}{R\partial\theta}\left(\frac{\rho h^3}{\sigma}\frac{\partial p}{R\partial\theta}\right)-\frac{\partial}{\partial z}\left(\frac{\rho h^3}{\sigma}\frac{\partial p}{\partial z}\right)+12\frac{\partial}{\partial t}(\rho h)+ \quad (3)$$
$$6\omega\frac{\partial}{\partial\theta}(\rho h)=\frac{d\dot{m}_k}{Rd\theta dz}$$

In light of the assumption that a flow in the gas film is isothermal, the gas viscosity in the Reynolds equation (3) can be treated as constant, and its density can be replaced by pressure. Moreover, introducing the dimensionless quantities $\xi = z / R$, $P = p / p_a$, $H = h / c$, $P^2=Q$ and $\tau = (\omega t) / (2\Lambda)$, these equations can be reduced to the form [1]:

$$-3H^2\left(\frac{\partial H}{\partial\theta}+\frac{\partial Q}{\partial\theta}+\frac{\partial H}{\partial\xi}+\frac{\partial Q}{\partial\xi}\right)-$$
$$H^3\left(\frac{\partial^2 Q}{\partial\theta^2}+\frac{\partial^2 Q}{\partial\xi^2}\right)+\frac{\Lambda}{P}H\frac{\partial Q}{\partial\theta}+$$
$$2\Lambda\frac{Q}{P}\frac{\partial H}{\partial\theta}+\frac{1}{P}H\frac{\partial Q}{\partial\tau}+2P\frac{\partial H}{\partial\tau} \quad (4)$$
$$=\frac{d\dot{m}}{2C^o d\theta d\xi}$$

The Reynolds equation is solved numerically to determine the pressure distribution of the air in the bearing gap at a given position of the journal with respect to the bush. In the case of the parallel axes of the journal and bush, the bearing gap is described by the eq (5)

$$H(\theta)=1-\varepsilon\cos(\theta-\theta_s)$$
$$\varepsilon=\frac{1}{c}\sqrt{e_x^2+e_y^2} \quad (5)$$
$$\theta_s=arctg\frac{e_x}{e_y}$$

The applied method of numerical integration of the Reynolds equation imposes on the air film an M x N grid with the coordinates θ, ξ as shown in Fig. 4. The values of the air pressure are determined in the grid points.

The alternating direction implicit scheme was used in the numerical solution of eq (4). The eq (1) and eq (2) of air flow through the feed system are solved along with the Reynolds eq (4).

The estimated pressure distribution in the gap between the journal and the bush enables evaluation of the components of the force acting between the journal and the bushing as the following integrals.

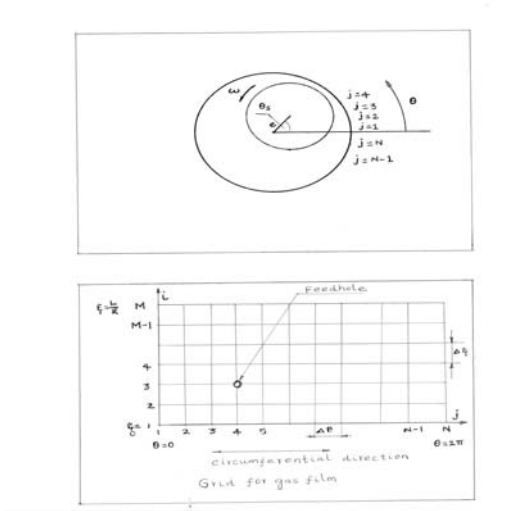

Fig. 4 Grid for air film

$$F_x(m\Delta\tau) = P_a R^2 \int_0^{2\pi} \int_0^{L/R} P^m(\xi,\theta).\cos\theta.d\xi.d\theta$$
$$F_y(m\Delta\tau) = P_a R^2 \int_0^{2\pi} \int_0^{L/R} P^m(\xi,\theta).\sin\theta.d\xi.d\theta \quad (6)$$

Such a calculation, conducted with an appropriately selected time step $\Delta\tau = 0.01$ to provide data for calculations of stiffness and damping coefficients, in the form of vectors of displacements, velocities and forces as shown below.

$$\begin{bmatrix} x(\tau) \\ x(\tau+2\tau) \\ x(\tau+4\tau) \\ . \\ . \\ . \\ x(\tau+2n\Delta\tau) \end{bmatrix}, \begin{bmatrix} \dot{x}(\tau) \\ \dot{x}(\tau+2\tau) \\ \dot{x}(\tau+4\tau) \\ . \\ . \\ . \\ \dot{x}(\tau+2n\Delta\tau) \end{bmatrix}, \begin{bmatrix} F_x(\tau) \\ F_x(\tau+2\tau) \\ F_x(\tau+4\tau) \\ \\ \\ \\ F_x(\tau+2n\tau) \end{bmatrix}, \begin{bmatrix} F_y(\tau) \\ F_y(\tau+2\tau) \\ F_y(\tau+4\tau) \\ \\ \\ \\ F_y(\tau+2n\tau) \end{bmatrix} \quad (7)$$

All the stiffness and damping coefficients are functions of the journal load, angular velocity and vibration frequency. For the given load F_z (i.e. the weight of micro turbine rotor), velocity Λ, and vibration frequency υ, the measurement of the displacements x and y, and the velocities $\dot{x}$ and $\dot{y}$ during one period T of the journal motion (in a steady state) carried out in time intervals $\Delta\tau = T / N$ to get the vectors F_{xx}, F_{yx}, F_{xy}, F_{yy} and x, y, $\dot{x}$, $\dot{y}$ [1], [7]. These vectors satisfy the relations given by

$$F_{xx} = C_{11}\, x + C_{13}\, x\, x + C_{15}\, x^2 + C_{17}\, x^2\, x + K_{11}\, x + K_{13}\, x^2 + K_{15}\, x^3,$$
$$F_{yx} = C_{21}\, x + C_{23}\, x\, x + C_{25}\, x^2 + C_{27}\, x^2\, x + K_{21}\, x + K_{23}\, x^2 + K_{25}\, x^3. \quad (8)$$
$$F_{xy} = C_{11}\, y + C_{13}\, y\, y + C_{15}\, y^2 + C_{17}\, y^2\, y + K_{11}\, y + K_{13}\, y^2 + K_{15}\, y^3,$$
$$F_{yy} = C_{21}\, y + C_{23}\, y\, y + C_{25}\, y^2 + C_{27}\, y^2\, y + K_{21}\, y + K_{23}\, y^2 + K_{25}\, y^3. \quad (9)$$

The stiffness and damping coefficients are calculated from eq (8) and eq (9) using orthogonalization procedure given by [1], [7], [14]. A dynamic analysis of the system whose elements are air bearings requires the knowledge of stiffness and damping coefficients for any velocities Λ and vibration frequencies υ of the rotor, from the required ranges of variations at the given load F_z of the bearing. To make it possible, identification of stiffness and damping coefficients for M selected values of Λ_i and N selected values of υ_i is carried out, which leads to the determination of the maps of the coefficients. In the neighborhood of the point (Λ, υ), these coefficients can be approximated by a Fourier series of variables Λ and υ [1], [7].

The equations that describe the motion of the rotor and bushes around their static equilibrium positions are written in the Cartesian co-ordinates x, y, and z. The dynamic reactions of the bearings to the displacement of the system under consideration from the static equilibrium position can be written in terms of the elastic and damping properties of the bearing air film found out using eq (8) and eq (9) [1]. The equations of free vibration of the rotor-bearing system (both cylindrical and conical modes) are the equations describing the equilibrium between inertia forces and dynamical forces of the reactions of the bearings and the construction supporting the bushes, acting on the rotor and bushes. The reduced system of equations is arrived from the linearized equations of free vibration by considering the symmetrical loading of the rotor. The solution of the reduced system of equations gives eigen values. Since the basic problem in calculating the eigen values lies in the dependence of the stiffness and damping coefficients of the air film on the frequency of the rotor free vibrations, which is an imaginary part of an unknown eigenvalue, therefore the calculations of the eigenvalues has been carried out by an iterative method of successive approximations [1].

Results and Discussion

Three different configurations of bearing having clearances in the range from 3 microns to 15 microns have been analyzed using the code developed. These are shown in Table 1 where all the dimensions are in μm and subscripts ($_1$), ($_2$) represent the dimensions of air bearing and air ring respectively.

Table 1 Dimensions of different air bearing configurations (micron)

Configuration	$c_1 = c_2$	$h_{k1}=h_{k2}$	$r_{o1}=r_{o2}$	$r_{d1}=r_{d2}$
1	3	250	100	15
2	9	750	300	45
3	15	1250	500	75

Air Film Pressure Distribution - All the configurations have been analyzed for the pressure distribution. Here only air pressure distribution for configuration 2 is discussed. Fig. 5 and 6 show the pressure distribution in the air film in between the journal and the bearing (inner bush) of the configuration 2 while the speed of rotation of the journal is 90010 rpm. Fig. 5 shows the pressure distribution at time 0.0109 sec where as the Fig. 6 shows the same at a later time, which is 0.0133 sec obtained from the simulation of the mathematical model. It is observed that there is a change in the pressure distribution with respect to time. It is also observed on both the figures that the pressure at both ends of the bearing is atmospheric (1 bar) satisfying imposed boundary condition, while the pressure distribution in the circumferencial direction satisfies the mass continuity condition. It is also seen that the pressure at '0' radian is equal to the pressure at '2π' radians. The pressures at the grid points where feedholes are provided are observed to be slightly less than the supply pressure due to the pressure drop in the feed holes.

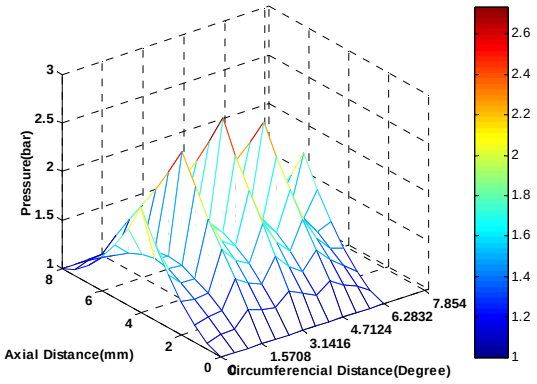

Fig. 5 Air Film Pressure Distribution, t=0.0109s, 90010 rpm, Configuration 2.

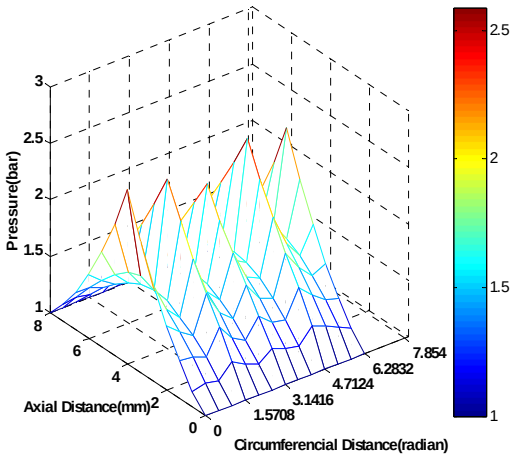

Fig. 6 Air Film Pressure Distribution, t=0.0133s, 90010 rpm, Configuration 2.

Dynamic Components of Bearing Load Capacity - Fig. 7 and Fig. 8 show the dynamic components of bearing load capacity in Newtons plotted against the time levels in seconds while the journal rotates at 90010 rpm for the bearing configuration 2. F_{xx} and F_{yx} are the components of bearing load capacity along the x and y axis respectively when the journal center follows the harmonic motion in the horizontal direction. F_{xy} and F_{yy} are the components of bearing load capacity along the x and y axis respectively when the journal center follows the harmonic motion in the vertical direction. These values are obtained by integrating the pressure distribution at different time intervals. It is observed that there is periodic variation in the values of force components after some initial transient period is completed which shows that the air bearing operation is at the steady state condition.

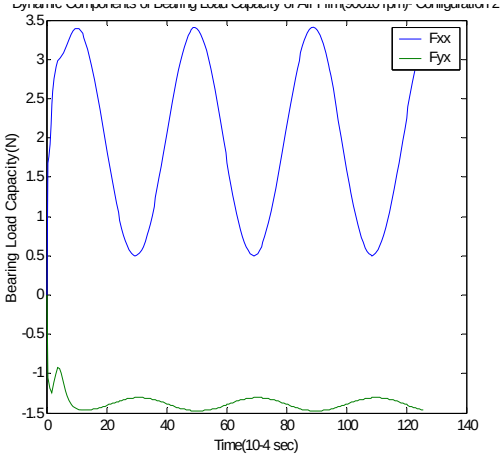

Fig. 7 Dynamic components of Bearing Load Capacity x=a sin (υτ), y=0.

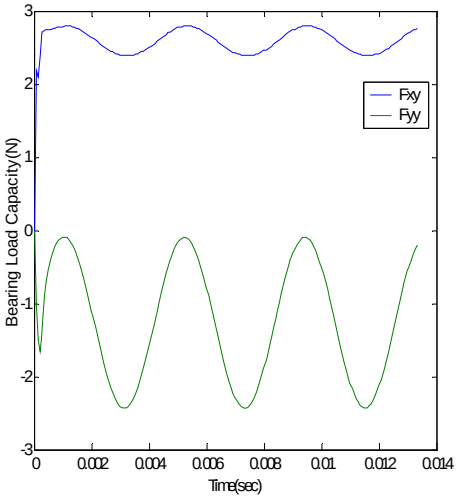

Fig. 8 Dynamic components of Bearing Load Capacity x=0, y= a sin (υτ).

Chamber Air Pressure and Mass Flow Through the Feedholes - Fig. 9 and Fig. 10 show the variation of chamber air pressure and mass flow through the feedhole number 1 respectively with respect to time while the journal rotates at 90010 rpm for the bearing configuration 2. It is observed that there is periodic variation in the air pressure in the chamber of the feedhole number 1. The maximum pressure is equal to 7 x 10^4 N/m^2 and the minimum pressure is equal to 6 x 10^4 N/m^2. In Fig. 10 it is observed that there is periodic variation in the mass flow. Whereas the average critical mass flow rate is 3.5 x 10^{-6} Kg/s the average value actual mass flow is around 3.2 x 10^{-6} Kg/s. It shows that the flow through the first feedhole is not choked. Similarly the results of the variation of chamber air pressure and mass flow through the feedhole nos.2, 3 and 4 have been arrived.

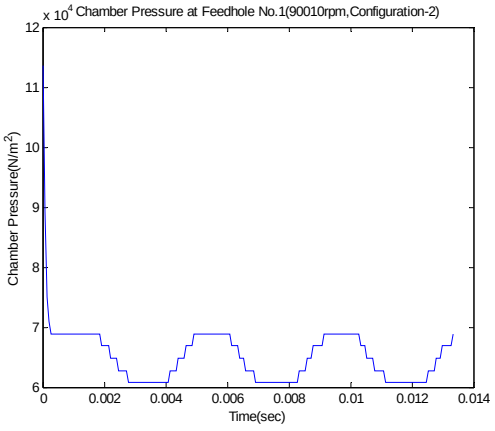

Fig. 9 Chamber Pressure at Feedhole No.1, 90010 rpm, Configuration 2

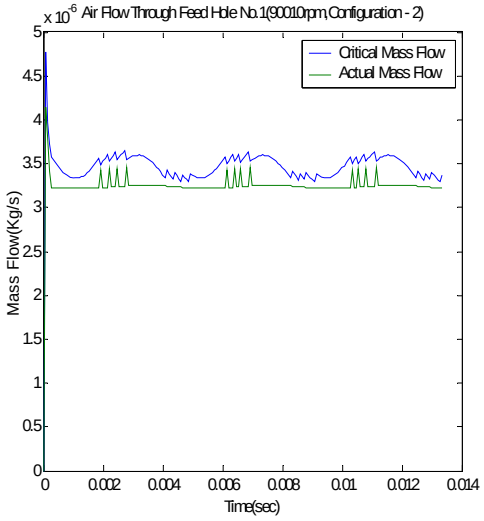

Fig. 10 Air Flow through Feedhole No.1, 90010 rpm, Configuration 2

Dimensionless Stiffness and Damping Coefficients - Fig. 11 and Fig. 12 show the linear dimensionless stiffness and damping coefficients of air bearing respectively as the functions of the frequency of motion of the journal ν for different values of the bearing number Λ for the bearing configuration 2. From these graphs the average value of the stiffness and damping coefficients of air bearing over the whole range of speed of operation and vibration frequencies can be obtained.

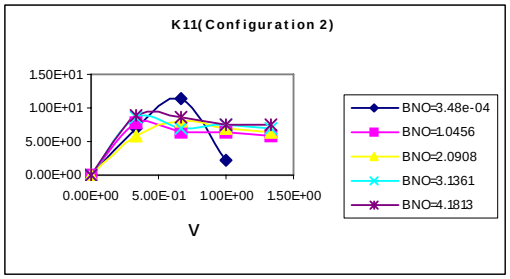

Fig. 11 Dimensionless Stiffness Coefficient K_{11}

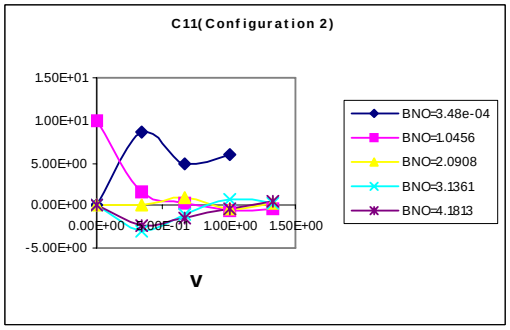

Fig. 12 Dimensionless Damping Coefficient C_{11}

Stability of Rotor-Air Bearing System - Here the bearing bushes are mounted directly in the fixed casing, a region of self-excited vibrations, which is unlimited from the top, spreads above a certain boundary rotational velocity. This situation changes when an elastic support consisting of linear springs K_p and the viscous dampers C_p is introduced between the bearing bushes and the casing, as the values of the stiffness and damping coefficients of the elastic support of the bushes (K_p and C_p) strongly influence the size of the instability regions [1]. Fig. 13 and 14 show the stability boundaries for cylindrical vibrations and conical vibrations respectively of the rotor for the bearing configuration 2. As can be seen, for each value of the stiffness coefficient K_p, the stable regions in which self-excited vibrations do not appear have a limited size. For small values (0.5) of K_p, the unstable regions exist for any value of the damping coefficient C_p. The stability boundaries show the ends of the unstable regions or the so-called always stable loop. For any value of the coefficients K_p and C_p selected inside the stable region there will be no self-excited vibrations appear during the system operation, irrespective of the rotational velocity value Λ or conversely these are the required values of stiffness and damping coefficients for the rotor-bearing system to be stable. The practical engineering solution of the elastic bush support is an air ring, which will produce the required stiffness and damping effect recommended by the values within the stability boundaries.

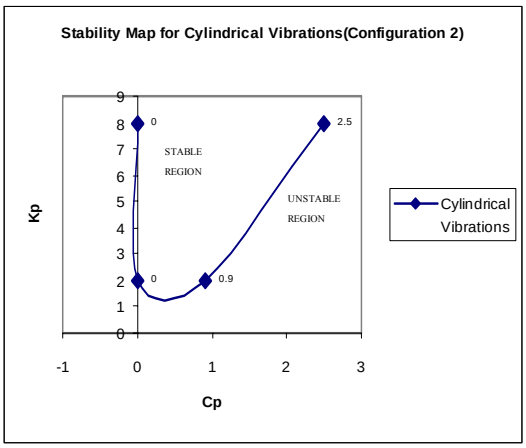

Fig. 13 Stability Map for Cylindrical Vibrations, Configuration 2.

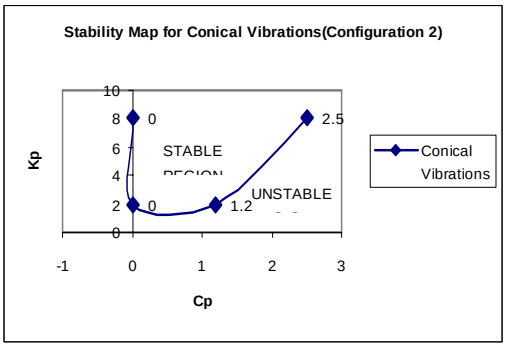

Fig. 14 Stability Map for Conical Vibrations, Configuration 2.

Air Ring Coefficients - As opposed to the arbitrarily selected constant values of the stiffness and damping coefficients K_p and C_p of the springs and dampers that support the systems considered for the development of the stability boundary maps, the stiffness and damping coefficients of the air rings depend on the frequency of vibrations ν of the bush, represented in the horizontal axes in Fig. 15 and Fig. 16. To increase in the value of the damping coefficient of the air ring, modification of the boundary conditions of the air film has been made by introducing longitudinal rubber seals that reduce circumferential airflow. It is observed from the Fig. 15 and 16 that all the stiffness coefficients in Fig. 15 (configuration 2) are inside the stable region as recommended by the Fig. 13 and Fig. 14. Also all the damping coefficients except the point indicated by –1.0 in the Fig. 16 (configuration 2), which corresponds to the frequency at the speed of 5010 rpm, satisfy the stability requirement of the Fig. 13 and 14. Thus the rotor will have stable operation in the range of speed from 5010 rpm to 1, 00,000 rpm under consideration only for the bearing configuration 2. The stiffness and damping coefficients of the air ring configurations 1 and 3 do not satisfy the stability requirements recommended by their respective stability maps.

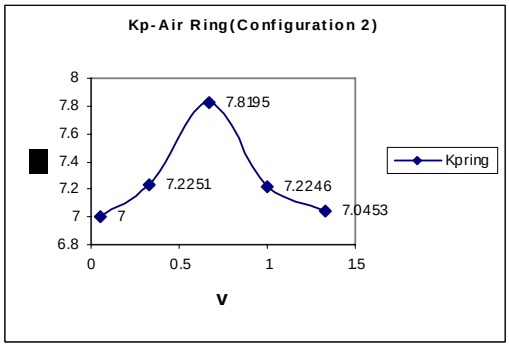

Fig. 15 Air Ring Stiffness Coefficient, Configuration 2

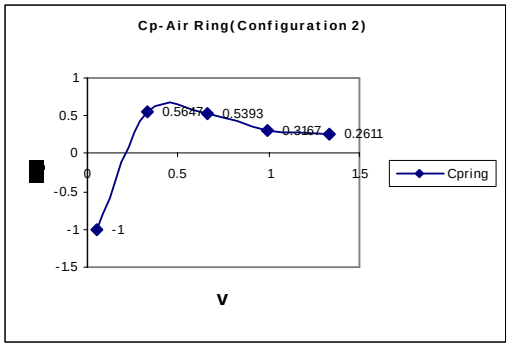

Fig. 16 Air Ring Damping Coefficient, Configuration 2

In Fig. 17 stiffness coefficients are plotted against damping coefficients for cylindrical and conical vibration. The regions of stable and unstable operation of the bearing are identified.

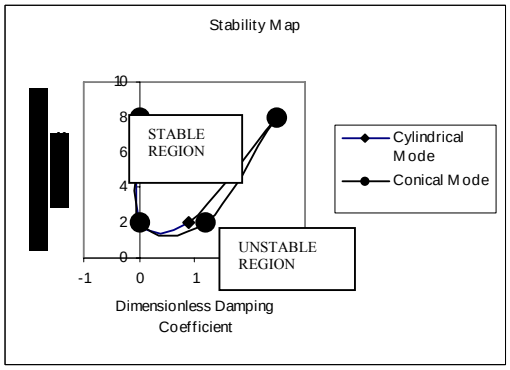

Fig. 17 Stability Map, Configuration 2

Conclusions

Three different configurations of bearing having clearances in the range from 3 microns to 15 micron have been analyzed using the code developed. The bearing having the geometry given below shows the stability over the whole range of speed under consideration.

Air Bearing	
Radius	5.0 mm.
Clearance	9.0 µm.
Chamber height	750.0 µm.
Feed hole radius	300.0 µm.
Orifice radius	45.0 µm.

Air ring	
Ring Radius	12.35 mm.
Clearance	9.0 µm.
Chamber height	750.0 µm.
Feed hole radius	300.0 µm.
Orifice radius	45.0 µm.

Fig. 17 shows the stability boundaries of the rotor for cylindrical and conical modes of vibration for the bearing configuration 2. The stiffness and damping coefficients of air ring of configuration 2 are shown in Figs. 15 and 16 for various vibration frequencies of rotor. As can be observed from these graphs, all the stiffness coefficients in Fig. 15 are inside the always-stable region in Fig. 17. Also all the damping coefficients except the point indicated by -1.0 in Fig. 16, which corresponds to frequency at the speed of 5010 rpm, satisfy the stability requirement of Fig. 17. Thus the rotor will have stable operation in the range of speed from 5010 rpm to 1, 00,000 rpm under consideration.

References

[1] Krzysztof Czolczynski, *Rotor Dynamics of Gas-Lubricated Journal Bearing Systems*, P.10-14, 92, 1999.

[2]. Czolczynski K., Kapitaniak T., Marynowski K., "Stability of Rotors Supported in Gas Bearings with Bushes Mounted in Air Rings", Wear, P.199, 1996.

[3] K Czolczynski, L.Brzeski and Z. Kazimierski, "High Stiffness Gas Journal Bearing under the Step Force", Wear, P-49-58, 1993.

[4] Lech Brzeski, Zbyszko Kazimierski, "High Stiffness Bearing", Journal of Lubrication Technology, P 520-525, 1979.

[5] E.S. Piekos, K.S. Breuer, "Pseudospectral Orbit Simulation of Nonideal Gas- Lubricated Journal Bearings for Micro fabricated Turbo machines", Journal of Tribology, P 604 – 609, 1999.

[6] G.H. Jang, Y.J. Kim, "Calculation of Dynamic Coefficients in a Hydrodynamic Bearing Considering Five Degrees of Freedom for a General Rotor-Bearing System", Journal of Tribology, P 499 – 505, 1999.

[7] K Czolczynski, "How to obtain stiffness and damping coefficients of gas bearings", Wear, P 265 – 275, 1996.

[8] Z. Kazimierski, J. Trojnarski, "Investigations of Externally Pressurized Gas Bearings with Different Feeding Systems", Journal of Lubrication Technology, P 59 – 64, 1980.

[9] Jeong-Bae Lee, Kyung-Woong Kim, "Effects of Synchronous Vibration of Bearing on Stability of Externally Pressurized Air Journal Bearings", Journal of Tribology, P 830 –834, 1999.

[10] G. Belforte, T. Raparelli V. Viktorov, "Theoretical Investigation of Fluid Inertia Effects and Stability of Self-Acting Gas Journal Bearings", Journal of Tribology, P 836 – 840, 1999.

[11] www.microturbine .com

[12] H. Heshmat, "Advancements in the Performance of Aerodynamic Foil Journal Bearings: High Speed and Load Capability", Journal of Tribology, P 287 – 292, 1994.

[13] V Castelli ,J.Pirvics, "Review of Numerical Methods in Gas Bearing Film Analysis", Journal of Lubrication Technology, P-777-792, 1968.

[14] Christoph W. Ueberhuber, *Numerical Computation (Methods, Software, and Analysis)*, Volume 2, Springer-Verlag Berlin Heidelberg, 1997.

M.Muruganandam,
Student, Thermal Engineering Branch,
Government College of Technology,
Coimbatore – 641 013, Tamil Nadu.
E-mail:muruganandammma@yahoo.co.in.

Mr.S.Nadarajan,
Selection Grade Lecturer, Mechanical
Engineering Department,
Government College of Technology,
Coimbatore – 641 013.
E-mail:nadarajan.s@rediffmail.com,
Ph.No:2432221 Extn:362.

Dr.S.Ramamurthy.
Scientist, CLOCTER, Propulsion
Department,
National Aerospace Laboratories,
Bangalore – 560 017,
E-mail:ramamurthy_srm@yahoo.com,
Ph.No:080-25051705, 25057787.